Analytical Formulas for the Coverage of Tunable Matching Networks for Reconfigurable Applications

Eyad Arabi, *Member, IEEE,* Kevin A. Morris, *Member, IEEE,* and Mark A. Beach, *Member, IEEE,*

***Abstract*—Tunable matching networks are essential components for agile radio frequency systems. To optimally design such networks, the total area they cover on the Smith chart needs to be determined. In this work, the coverage areas of typical matching networks have been determined analytically for the first time. It has been found that the coverage area is encompassed by up to five arcs. Analytical expressions for the centers and radii for these arcs have been derived. The theoretical analysis is provided for four typical matching networks and verified by circuit simulation and measured data. Moreover, a dynamically load-modulated power amplifier has been designed using the presented theoretical techniques, which demonstrates a measured improvement in the power added efficiency of up to 5% in the frequency range of (0.8 - 0.9) GHz.**

***Index Terms*—Smith chart, tunable matching networks, power amplifiers, re-configurable, dynamic load modulation**

I. Introduction

RECONFIGURABLE wireless transceivers are becoming crucial for future systems such as long-term evolution (LTE) and LTE-advanced. Such systems are required to be frequency agile to enable optimal utilization of the congested frequency spectrum. Therefore, these systems require tunable components like antennas, filters, and matching networks (MN).

Beside frequency agile systems, tunable MN are being used heavily for applications such as tunable/wideband antennas [1], efficiency-enhanced and load-sensitive power amplifiers (PAs) [2], [3], and range-adaptive wireless power transfer [4]. One of the main parameters the RF designer needs to know about a tunable MN, is the set of all complex impedances that can be matched to a specific load (typically 50 Ω). This set defines what is known as the coverage of the MN.

The Smith chart continues to serve as an indispensable tool for the analysis and visualization of complex loads and reflection coefficients [5]. Compared to the complex impedance-plane, the Smith chart is a superior tool because multiple quantities can be read directly, such as the complex impedance and admittance and the reflection coefficient. Therefore, the coverage of MNs defined in the complex plane of the Smith chart is of great benefit. This is particularly useful for PAs because the coverage can be plotted along with other criteria such as load-pull contours, noise circles, gain circles, etc.

In [6]–[11] the boundaries have been presented using simulations, which are less legible, do not indicate the limits of the tuning elements, and do not provide any physical insight about the networks. In [12], theoretical formulas have been presented; however, they provide the coverage for discrete impedance points (states) and do not give the continuous coverage, and they are not directly related to the tunable capacitors commonly used in matching networks. Even though the formulas in [13]–[15] can produce the coverage for the full dynamic range, they are presented for the complex rectangular plane, not the Smith chart and for Π networks only. In this work, the coverage areas of four of the commonly used networks have been thoroughly investigated. Theoretical formulas have been derived for the loci of the closed boundaries of the coverage areas. These formulas are derived for the complex space of the reflection coefficient rather than the impedance and can, therefore, be plotted directly on the Smith chart. It is assumed that the MN is connected to a resistive load at one end, and the reflection coefficient seen looking towards the other end defines the coverage area as illustrated in Fig. 1 (a). This configuration is different from the one in [6]–[10], [12] where a resistive load is connected at one end with the other end conjugately matched to a known impedance. The configuration used here is particularly suitable for PAs where conjugate matching is not necessarily required. The theoretical analysis has been verified by circuit simulation as well as measured data, which agrees well with the theory.

The theoretical formulas presented here are compact; therefore, very practical for use in CAD tools and provide a useful instrument for the analysis of tunable MN.

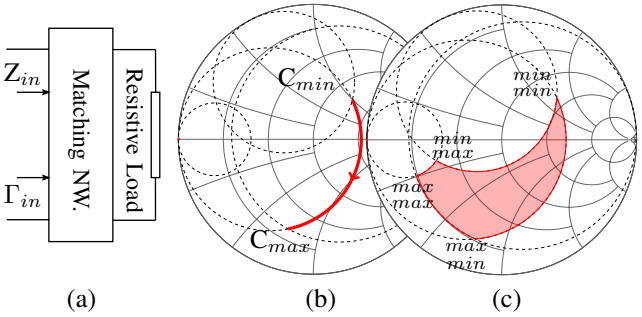

Fig. 1. Illustration of the boundary of the coverage area. (a) Problem description. (b) Networks with only one tunable element. (c) Networks with two tunable elements.

II. Theory

The coverage of a tunable MN can be defined as the set of all complex impedances that can be matched to a specified load at a particular frequency. If the MN has only one tunable

Manuscript received December 1st, 2016; revised January 21st, 2017; accepted March 21st, 2017.

The authors are with the department of Electrical and Electronic Engineering, University of Bristol, BS8 1UB, Bristol, UK. E-mail: {eyad.arabi, kevin.morris}@bristol.ac.uk

component, its coverage will be a linear path as shown in Fig. 1(a). If the MN has more than one tunable component, then the coverage is typically an area on the Smith chart as shown in Fig. 1(b). The boundary of such area will be referred to here as the *coverage boundary* and is always a closed path. In this work, MNs with two tunable elements (C_1 and C_2) are analyzed. Nevertheless, the theoretical methods introduced here can be applied to networks with a higher number of tunable elements, but the formulas become large and less practical. The two elements are not necessarily identical and can take any values between C_{min} and C_{max}. The load is assumed to be pure resistive taking a value of Y_0 Ω^{-1}.

The first step of the analysis is to sweep both capacitors within their limits and observe the area covered by the matching network. It has been found that the coverage area is bounded by four arcs. The first two arcs are plotted by letting $C_1 \in \{C_{min}, C_{max}\}$ and C_2 takes all the real numbers between C_{min} and C_{max}. The remaining two arcs are plotted by letting $C_2 \in \{C_{min}, C_{max}\}$ and C_1 takes all the real numbers between C_{min} and C_{max}. These four arcs are parts of circles which can be completely plotted by extending the limits of the capacitors to -∞ and ∞. For lossless networks, all of these circles are tangent to the $|\Gamma| = 1$ circle. The value of the capacitor at the tangent point can be calculated by solving for Y_{in} that falls on the $|\Gamma| = 1$ circle according to:

$$|\Gamma| = \left|\frac{Y_0 - Y_{in}}{Y_0 + Y_{in}}\right| = 1 \tag{1a}$$

$$|Y_0 - Y_{in}| = |Y_0 + Y_{in}|, \tag{1b}$$

which is satisfied only when the real part of Y_{in} is either zero or ∞ corresponding to either an open or a short circuit, respectively. A short circuit can be achieved by a shunt branch with zero impedance (if the branch has only a capacitor the capacitance can be set to ∞). An open circuit, on the other hand, can be achieved by a series branch with infinitely large impedance (if the branch has only a capacitor, its value can be set to zero).

The centers and radii of the four circles can be calculated from the tangent point and *any* other point. If the tangent point is denoted A(x_A, y_A) and the other point is denoted B(x_B, y_B), the center (x_c, y_c) and radius (R_c) of the circle can be calculated, as derived in Appendix B, by:

$$x_c = \frac{x_A\left(x_B^2 - x_A^2 + y_B^2 - y_A^2\right)}{2\left(-x_A^2 - y_A^2 + x_A x_B + y_A y_B\right)}, \tag{2a}$$

$$y_c = \frac{y_A\left(x_B^2 - x_A^2 + y_B^2 - y_A^2\right)}{2\left(-x_A^2 - y_A^2 + x_A x_B + y_A y_B\right)} \quad \text{and} \tag{2b}$$

$$R_c = \sqrt{(x_c - x_A)^2 + (y_c - y_B)^2}, \tag{2c}$$

respectively.

The four circles for a hybrid network are plotted in Fig. 2 together with the coverage area using the theoretical formulas presented here and verified by a commercial simulator. It can be observed that a fifth circle (referred to in the figure as C_2') is also needed to complete the boundary. This circle is a function of the inductors and transmission lines as well as the frequency and is referred to here as the *auxiliary circle*. For given values of these parameters, impedances inside the auxiliary circle can not be matched even if the values of the tunable capacitors extend from -∞ to ∞ [16]. As illustrated in Fig. 2, the auxiliary circle is traced when C_1 is swept while C_2 is assigned a critical value (C_2'), which resonates with the transmission line when $C_2 = Y_0/\omega\tan(\theta)$. Formulas for C_2' are derived for various network topologies in the following section. The auxiliary circle becomes part of the boundary only if C_2' falls within the tuning range of C_2. Since the auxiliary circle defines a forbidden region, the constant circles of $C_{1,min}$ and $C_{1,max}$ can not intersect with this circle, but only shares a single point with it and thus the three circles must be tangent.

In the following sections, four different matching networks are analyzed and the derived formulas to calculate the five circles are presented.

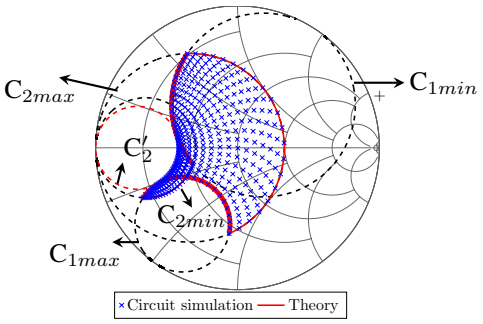

Fig. 2. Illustration of the four main circles and the auxiliary circle that form the boundary of the matching network. The coverage is verified by a commercial simulator.

A. T-Matching Network

A lumped T-type MN is illustrated in Fig. 3(a). To analyze this network as mentioned in the previous section, the coordinates of the points of the C_1 and C_2 circles need to be calculated.

1) C_1 variable and C_2 constant: For the first case, $C_2 \in \{C_{min}, C_{max}\}$ while C_1 can take any real number between these two limits. To plot the complete circle, however, we will let $C_1 \in \mathbb{R}_{\geq 0}$. The first point to be calculated is the point at which this circle is to the outer circle ($|\Gamma| = 1$). This point is referred to as point A and corresponds to $C_1 = 0$. Using this value, the input admittance (Y_{in}) becomes infinite, and the real and imaginary parts of the input reflection coefficient (Γ_{in}) are

$$x_{A1} = 1 \qquad \text{and} \tag{3a}$$

$$y_{A1} = 0. \tag{3b}$$

For the second point (point B), C_1 is assumed to take an infinitely large value, which corresponds to an RF short circuit. Using this assumption, the real and imaginary values of Y_{in} can be calculated as:

$$\Re\{Y_{in}\} = \frac{Y_0\left(\omega^2 L C_2\right)^2}{\left(\omega^2 L C_2\right)^2 + \left(Y_0 \omega L\right)^2} \tag{4a}$$

and

$$\Im\{Y_{in}\} = \frac{\omega L\left(-\omega^2 C_2^2 - Y_0^2 + Y_0^2\omega^2 L C_2\right)}{\left(\omega^2 L C_2\right)^2 + \left(Y_0\omega L\right)^2}, \quad (4b)$$

from which the real and imaginary values of Γ_{in} are:

$$x_{B1} = \frac{-\left(\Re\{Y_{in}\}\right)^2 + Y_0^2 - \left(\Im\{Y_{in}\}\right)^2}{\left(\Re\{Y_{in}\} + Y_0\right)^2 + \left(\Im\{Y_{in}\}\right)^2} \quad \text{and} \quad (5a)$$

$$y_{B1} = \frac{-2Y_0\Im\{Y_{in}\}}{\left(\Re\{Y_{in}\} + Y_0\right)^2 + \left(\Im\{Y_{in}\}\right)^2}, \quad (5b)$$

respectively.

The coordinates of points A and B can be directly used in equation (2) to calculate the centers and radii of the circles. Two circles are obtained: one for $C_2 = C_{min}$ and another for $C_2 = C_{max}$.

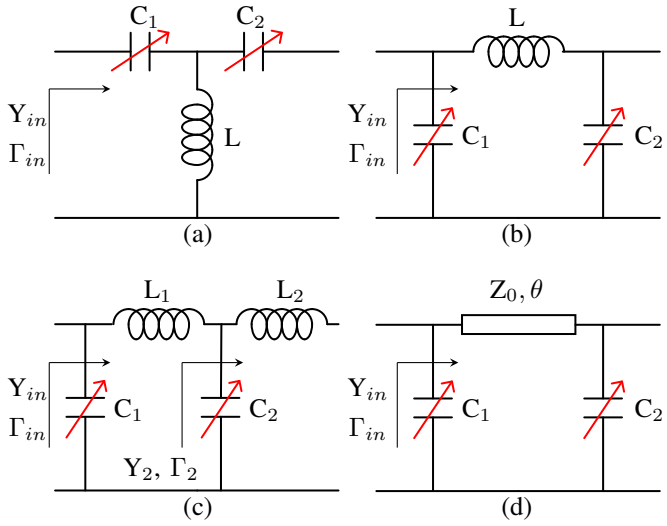

Fig. 3. Schematics of the four topologies analyzed in this work. (a) T-type. (b) Π-type. (c) Ladder-type. (d) Hybrid Π. $\Gamma_{in} = x + jy$ is the input reflection coefficient and Y_{in} is the input admittance.

2) C_1 constant and C_2 variable: For this case $C_1 \in \{C_{min}, C_{max}\}$ while $C_2 \in \mathbb{R}_{\geq 0}$. The first point in this case corresponds to $C_2 = 0$, which gives the following values of the real and imaginary of Γ_{in}

$$x_{A2} = \frac{Y_0^2\left(1 - \omega^2 L C_1\right)^2 - \left(\omega C_1\right)^2}{Y_0^2\left(1 - \omega^2 L C_1\right)^2 + \omega^2 C_1^2} \quad (6a)$$

$$y_{A2} = \frac{-2\omega Y_0 C_1\left(1 - \omega^2 L C_1\right)}{Y_0^2\left(1 - \omega^2 L C_1\right)^2 + \omega^2 C_1^2}. \quad (6b)$$

This point has a unity magnitude regardless of the value of C_1 and, therefore, always lies on the outer circle. For the second point, the assignment: $C_2 = \infty$ is used and the real and imaginary values of Γ_{in} are:

$$x_{B2} = \frac{Y_0^2\left(1 - 2\omega^2 L C_1\right) + \omega^2\left(Y_0^2 L^2 - C_1^2\right)}{Y_0^2\left(1 - 2\omega^2 L C_1\right)^2 + \omega^2\left(Y_0^2 L + C_1\right)^2} \quad (7a)$$

and

$$y_{B2} = \frac{\omega Y_0\left(Y_0^2 L - C_1\right)\left(1 - 2\omega^2 L C_1\right) - \omega Y_0\left(Y_0^2 L + C_1\right)}{Y_0^2\left(1 - 2\omega^2 L C_1\right)^2 + \omega^2\left(Y_0^2 L + C_1\right)^2}, \quad (7b)$$

respectively. These two points can be used in equation (2) to calculate the centers and radii of the circles of $C_1 = C_{min}$ and $C_1 = C_{max}$.

3) Auxiliary Circle: The T-type network can match impedances up to a maximum resistance. The first derivative of the real part of the input impedance with respect to C_2 can be used to determine the value of C_2 that provides this resistance as derived in Appendix B-B, and given by:

$$C_2' = \frac{1}{\omega^2 L}. \quad (8)$$

The necessary condition for the auxiliary circle to be part of the boundary is for this value to fall within the limits of C_2:

$$C_{min} < C_2' < C_{max}. \quad (9)$$

The auxiliary circle itself can be plotted by using the value of C_2 defined in (8) with the formulas of section II-A1

In Fig. 4-(a), an illustration of the boundary of a T-type MN is illustrated for $L = 10$nH and frequencies of 0.5 GHz, 1.2 GHz, and 2.5 GHz. The complete circles are also included for the case of 1.2 GHz.

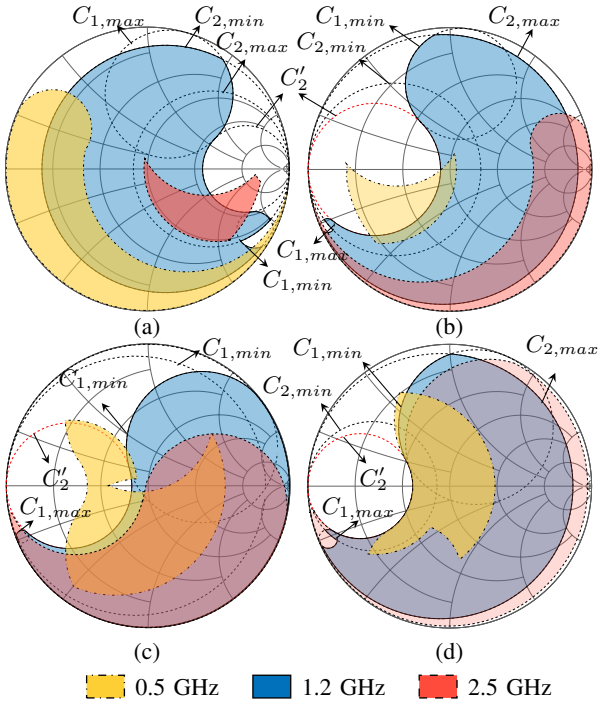

Fig. 4. Illustration of the boundary at three different frequencies with the values: C_{min}=0.5 pF, C_{max}=15 pF, θ=50, Z_0=50 Ω, L_T=10 nH, L_Π=6.2 nH and L_1=L_2 = 13 nH. (a) T-Network. (b) Π-Network. (c) Ladder Network. (d) Hybrid-Π Network.

B. Π-Type Matching Network

A typical Π-Type MN is illustrated in Fig. 3(b). It consists of an inductor between two shunt capacitors. The analysis of this network can be performed by the same method used in the previous section.

1) C_1 variable and C_2 constant: For this case, the coordinates of the first point are calculated by putting $C_1 = \infty$. At this case the input of the MN appears to have a zero impedance and, therefore, the real and imaginary values of Γ_{in} are

$$x_{A1} = -1 \qquad \text{and} \tag{10a}$$
$$y_{A1} = 0 \tag{10b}$$

respectively.

For the second point, C_1 is assigned a value of zero and the real and imaginary parts of the input admittance (Y_{in}) are

$$\Re\{Y_{in}\} = \frac{Y_0\left(1-\omega^2 LC_2\right)+\omega^2 Y_0 LC_2}{\left(1-\omega^2 LC_2\right)^2+\left(\omega Y_0 L\right)^2} \tag{11a}$$

and

$$\Im\{Y_{in}\} = \frac{\omega C_2\left(1-\omega^2 LC_2\right)-\omega Y_0^2 L}{\left(1-\omega^2 LC_2\right)^2+\left(\omega Y_0 L\right)^2} \tag{11b}$$

respectively. The real and imaginary parts of the reflection coefficient (x_{B1} and y_{B1}) can be calculated from Y_{in} using (5).

2) C_1 constant and C_2 variable: For the first point of this case, C_2 is assigned a value of ∞ (RF short circuit). The real and imaginary parts of Γ_{in} are calculated to be

$$x_{A2} = \frac{\left(\omega Y_0 L\right)^2-\left(1-\omega^2 LC_1\right)^2}{\left(\omega Y_0 L\right)^2+\left(1-\omega^2 LC_1\right)^2} \quad \text{and} \tag{12a}$$
$$y_{A2} = \frac{2\omega Y_0 L\left(1-\omega^2 LC_1\right)}{\left(\omega Y_0 L\right)^2+\left(1-\omega^2 LC_1\right)^2} \tag{12b}$$

respectively. This point has a unity magnitude regardless of the value of C_1. For the second point, C_2 is assigned a value of zero. The real and imaginary parts of Y_{in} are:

$$\Re\{Y_{in}\} = \frac{Y_0}{1+\left(\omega Y_0 L\right)^2}, \quad \text{and} \tag{13a}$$
$$\Im\{Y_{in}\} = \frac{\omega\left(C_1 - Y_0^2 L + C_1\left(\omega Y_0 L\right)^2\right)}{1+\left(\omega Y_0 L\right)^2}, \tag{13b}$$

respectively. These values can be used to calculate the coordinates of Γ_{in} using (5).

3) The Auxiliary Circle: This network can match impedances up to a maximum conductance. The first derivative of the real part of the input admittance with respect to C_2 can be used to calculate the value of C_2 that produces this conductance as shown in Appendix B-A and given by the following formula:

$$C_2' = \frac{1}{\omega^2 L}. \tag{14}$$

The condition for the auxiliary circle to be part of the boundary is the same as the one defined for the T-network in equation (9), and the auxiliary circle can be plotted by using the value of C_2' calculated in (14) with the formulas of section II-B1.

In Fig. 4-(b), an illustration of the boundary of a Π-type MN is illustrated for $L = 6.2$ nH and at frequencies of 0.5 GHz, 1.2 GHz, and 1.5 GHz. The complete boundary circles are also plotted.

C. Ladder Matching Network

This type of MN is illustrated in Fig. 3(c). It consists of two L-sections connected in series. The analysis of this network is presented in the following sections.

1) C_1 variable and C_2 constant: For this case, C_1 is assigned the values of zero and ∞. When $C_1 = \infty$ the real and imaginary parts of Γ_{in} are clearly given by:

$$x_{A1} = -1 \qquad \text{and} \tag{15a}$$
$$y_{A1} = 0 \tag{15b}$$

respectively. When $C_1 = 0$, on the other hand, the real and imaginary parts of Y_{in} are calculated as:

$$\Re\{Y_{in}\} = \frac{\Re\{Y_2\}\left(1-\omega\Im\{Y_2\}L_1\right)+\omega\Re\{Y_2\}\Im\{Y_2\}L_1}{\left(1-\omega\Im\{Y_2\}L_1\right)^2+\left(\omega\Re\{Y_2\}L_1\right)^2} \tag{16a}$$

and

$$\Im\{Y_{in}\} = \frac{\Im\{Y_2\}\left(1-\omega\Im\{Y_2\}L_1\right)-\omega\left(\Re\{Y_2\}\right)^2 L_1}{\left(1-\omega\Im\{Y_2\}L_1\right)^2+\left(\omega\Re\{Y_2\}L_1\right)^2}, \tag{16b}$$

respectively, where

$$\Re\{Y_2\} = \frac{Y_0}{1+\left(\omega Y_0 L_2\right)^2}, \quad \text{and} \tag{16c}$$
$$\Im\{Y_2\} = \frac{\omega\left(C_2\left(1+\left(\omega Y_0 L_2\right)^2\right)-Y_0^2 L_2\right)}{1+\left(\omega Y_0 L_2\right)^2}. \tag{16d}$$

$\Re\{Y_{in}\}$ and $\Im\{Y_{in}\}$ can be used to calculate the real and imaginary parts of Γ_{in} using equation (5).

2) C_1 constant and C_2 variable: For this case C_2 is assigned zero and ∞. For $C_2 = \infty$, which is an RF short circuit, the real and imaginary parts of Γ_{in} are given respectively by

$$x_{A2} = \frac{\left(\omega Y_0 L_1\right)^2-\left(1-\omega^2 L_1 C_1\right)^2}{\left(1-\omega^2 L_1 C_1\right)^2+\left(\omega Y_0 L_1\right)^2}, \quad \text{and} \tag{17a}$$
$$y_{A2} = \frac{2\omega Y_0 L_1\left(1-\omega^2 L_1 C_1\right)}{\left(1-\omega^2 L_1 C_1\right)^2+\left(\omega Y_0 L_1\right)^2}. \tag{17b}$$

This point is on the outer circle of the Smith chart because it has a magnitude of one regardless of the value of C_1. For the second point, $C_2 = 0$ and the real and imaginary parts of Y_{in} are given respectively by:

$$\Re\{Y_{in}\} = \frac{Y_0}{1 + \left(\omega Y_0 \left(L_1 + L_2\right)\right)^2} \tag{18a}$$

and

$$\Im\{Y_{in}\} = \frac{\omega C_1 - \omega Y_0^2 \left(L_1 + L_2\right)\left(1 - \omega^2 C_1 \left(L_1 + L_2\right)\right)}{1 + \left(\omega Y_0 \left(L_1 + L_2\right)\right)^2}. \tag{18b}$$

3) Auxiliary Circle: This network can also match impedances up to a maximum conductance. The value of C_2' is calculated in Appendix B-C and is given by:

$$C_2' = \frac{1}{\omega^2 L_1} + \frac{Y_0^2 L_2}{1 + \left(Y_0 \omega L_2\right)^2}. \tag{19}$$

The condition for the auxiliary circle to be part of the boundary is given by equation (9), and the auxiliary circle can be plotted by using the value of C_2' produced in (19) above with the formulas of section II-C1.

In Fig. 4-(c) the coverage circles together with the associated boundary are plotted for values of $L_1 = L_2$=13 nH, and frequencies of 0.5 GHz, 1.2 GHz, and 2.5 GHz.

D. Hybrid-Π Matching Network

The last network is a hybrid-Π, which consists of a transmission line with two shunt variable capacitors at its ends as illustrated in Fig. 3-(d). This network is analyzed in the following sections.

1) C_1 variable and C_2 constant: In the first case C_2 is fixed and C_1 is a variable. The two points are obtained as in the previous sections by assigning zero and ∞ to C_1. For the latter the real and imaginary parts of Γ_{in} are:

$$x_{A1} = -1 \qquad \text{and} \tag{20a}$$
$$y_{A1} = 0. \tag{20b}$$

For the second point, C_1 is assigned a value of zero. The real and imaginary parts of Y_{in} are then calculated as

$$\Re\{Y_{in}\} = \frac{Y_0^2 \left[Y_0 - \omega C_2 \tan\theta + \tan\theta \left(\omega C_2 + Y_0 \tan\theta\right)\right]}{\left(Y_0 - \omega C_2 \tan\theta\right)^2 + \left(Y_0 \tan\theta\right)^2} \tag{21a}$$

and

$$\Im\{Y_{in}\} = \frac{Y_0 \left[\left(\omega C_2 + Y_0 \tan\theta\right)\left(Y_0 - \omega C_2 \tan\theta\right) - Y_0^2 \tan\theta\right]}{\left(Y_0 - \omega C_2 \tan\theta\right)^2 + \left(Y_0 \tan\theta\right)^2}. \tag{21b}$$

These values can be used in (5) to calculate the real and imaginary parts of Γ_{in}, which can be used together with the first point to calculate the centers and radii of the circles associated with C_1.

2) C_1 constant and C_2 variable: In this case, C_1 is fixed at either $C_{1,min}$ or $C_{1,max}$ while C_2 is a variable. The two circle points can be calculated by assigning zero and ∞ to C_2. When $C_2 = \infty$ the real and imaginary parts of Y_{in} are given by

$$\Re\{Y_{in}\} = 0, \qquad \text{and} \tag{22a}$$
$$\Im\{Y_{in}\} = \omega C_1 - \frac{Y_0}{\tan\theta}, \tag{22b}$$

where Y_0 is the characteristic admittance of the line, which is also the same as the admittance of the load. Using these values and equation (5), the real and imaginary parts of Γ_{in} can be directly calculated.

In a similar way when $C_2 = 0$ the real and imaginary parts of Y_{in} are given by:

$$\Re\{Y_{in}\} = Y_0, \qquad \text{and} \tag{23a}$$
$$\Im\{Y_{in}\} = \omega C_1. \tag{23b}$$

Once more, equation (5) can be used to calculate the real and imaginary parts of Γ_{in}. From these two points, the centers and radii of the circles associated with C_1 can be directly calculated using the relations in section II.

3) Auxiliary Circle: In this case the maximum conductance that can be matched is a function of the transmission line parameters and C_2. The value of C_2 that gives the maximum conductance is derived in Appendix B-D and is given by:

$$C_2' = \frac{Y_0}{\omega \tan(\theta)}, \tag{24}$$

and the necessary condition for the auxiliary circle to be part of the boundary is given by (9). The auxiliary circle can be plotted by using the value of C_2' calculated in (24) and the formulas of section II-D1. The coverage for three different frequencies are illustrated in Fig. 4-(d).

III. Implementation of the Theoretical Results

A. Connecting the Boundary Area

All five circles of the boundary coverage can be plotted using the formulas presented in the previous section. Since these circles intersect at multiple points, it is necessary to provide a systematic way to identify and connect the arcs of the boundary area. As illustrated in Fig. 5 (c), four points can be identified for all the combinations of the maximum and minimum values of the two capacitors. If the auxiliary circle is part of the boundary, two more points are required making a total of six points. To uniquely define any arc, the starting and ending points together with its center and radius are not sufficient, and a third point is needed. This point can be selected arbitrarily as far as it corresponds to capacitances between the minimum and maximum values. For convenience, however, the median of the capacitances is chosen. Given this information, the arcs can be plotted as detailed in Appendix C.

B. Design Guidelines

The design and optimization of tunable MNs depends highly on the application at hand. However, important general rules can be derived based on the theoretical analysis presented in this work. The first task in the design is usually the selection of the most suitable network topology. Apart from other application-dependent requirements, the main factor in the selection is the range of capacitance required. The topology that provides the required coverage using capacitors with the smallest range should be favored. Also, the network that offers smaller capacitances should be selected because the quality factors of variable capacitors is highest at their lowest values. Once a suitable network is selected it can be optimized using the tool presented in this work with the following steps:

1) Use the formulas in Appendix B to calculate the values of L or θ to guarantee coverage of the maximum conductance (resistance for the case of the T-NW).
2) Calculate C_2' using L or θ from the previous step.
3) Ensure that $C_{2,min} < C_2' < C_{2,max}$ by re-selecting L and θ. This will guarantee wide boundary coverage because C_2' defines a critical limit.
4) Since the auxiliary circle is included in the boundary by design, select the value of $C_{2,min}$ ($C_{2,max}$ for the case of the T-NW) close to C_2' because values of $C_{2,min}$ below and above C_2' result in identical impedances and therefore duplicate coverage as shown in Fig. 5 (a) and (b). This condition can be derived for the case of the Π NW, without loosing generality, by assigning $C_2 = C_2' \pm C_\Delta$ in equation (33) to give:

$$\Re\{Y_{in}\} = \frac{Y_0}{(\omega L)^2\,[Y_0^2 + (\pm\omega C_\Delta)^2]}, \qquad (25)$$

which clearly does not depend on the sign of C_Δ. Therefore, as far as $C_{2,min} < C_2'$, a region on the coverage area is covered twice as illustrated in Fig. 5 (b) (this area can also be observed in Fig. 2 as the densely covered region).
5) After selecting L, θ and $C_{2,min}$ (or $C_{2,max}$ for the case of the T), the rest of the parameters can be selected according to the required coverage.

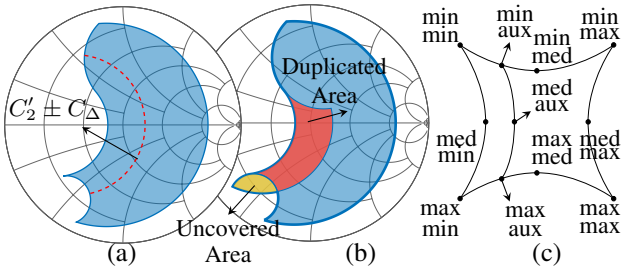

Fig. 5. (a) Coverage area with $C_{2,min}$=C_2'. (b) Coverage area with $C_{2,min} < C_2'$. The duplicate area is covered twice for the case of (b), while the uncovered area is dropped for the case of (a). (c) Illustration of the five arcs and 11 points of the boundary. Each point is defined by the values of C_1 and $C_2 \in$ {min, max, med, aux}, which refer to the minimum, maximum, median, and C_2', respectively.

IV. Measurements and Discussions

To verify the theoretical formulas presented in the previous sections, prototypes for all four matching networks have been fabricated and measured. The RT/Duroid® 5880 substrate has been used with a thickness of 0.508 mm. The printed circuit boards were fabricated using Laser etching. For the tunable capacitor, the varactor BB388 from Infineon has been used. The fabricated circuits are shown in Fig. 7.

A. Measurements

First, the C-V characteristics of the varactor have been measured at the frequencies of interest. To take the measurement, a circuit board has been fabricated for the varactor with one end shorted to the ground. The capacitance has been extracted from the S_{11} measurement. In Fig. 6 the capacitance is plotted against the reverse voltage for various frequency points. A model provided by the manufacturer has been used to generate the simulated results presented in the figure. Since the used varactor is packaged, its capacitance changes with frequency due to the effects of the package parasitics. These parasitics originate from the wire-bonds and are mostly inductive resulting in a self-resonant-frequency, which can be clearly observed in the figure.

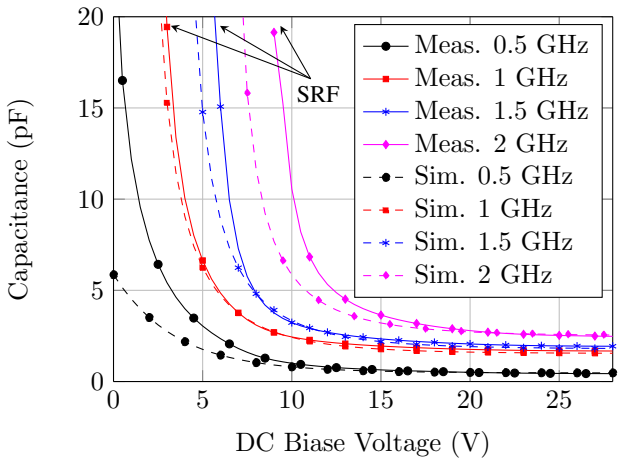

Fig. 6. Measured and simulated capacitance of the varactor against the bias voltage at multiple frequencies.

Lumped components in the theoretical analysis presented in the previous sections are assumed to be ideal, and the entire networks are assumed to be infinitesimally small. These assumptions can not be realized in practice as surface mounted components (SMT) are not ideal, and the circuits have to be large enough for fabrication and measurement reasons. To obtain results comparable with the ideal theory, the circuits have been made as small as possible. Moreover, the input/output connectors and feed lines have been de-embedded from the measured S-parameters. The parasitic effects of the solder and small conductive patterns connecting the SMT components have not been de-embedded. However, these parasitic effects are proportional to the frequency and can be reduced considerably by lowering the test frequency. For this reason, a relatively low frequency of 500 MHz has been chosen to

verify the theory. From the good match between the theory and measurement, it can be concluded that if the circuits are small enough, and the parasitics reduced (integrated designs), the theory can also be verified for higher frequencies.

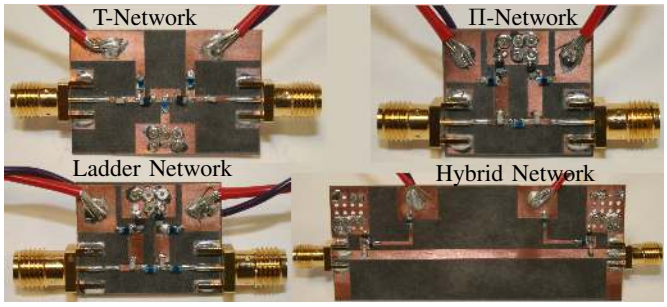

Fig. 7. Photographs of the fabricated prototypes.

The measurements of the matching networks have been performed using a digital power supply (TTi MX100TP) and a network analyzer (Keysight N5242A) both controlled by a PC. The DC voltages of the two varactors have been swept from 2 to 28 V in steps of 0.5 V. The measurement has been automated, and a total of 2809 points have been measured for each frequency. The results are compared to the theory for all matching networks in Fig. 8.

B. Analysis and Discussion

From Fig. 8 (a) a good agreement between theory and measurements can be observed with the four arcs clearly identifiable from the measurements. The minor discrepancy is mainly due to the ideal components assumed in the theoretical analysis. It can also be observed that the points at the edge of the chart, which are predicted by the theory, are not obtained in the measurement. As proofed by equation (1), when the matched impedance is on or close to the outer circle, its real part should be either zero or ∞. This condition can only be satisfied if the matching network is purely reactive, which is not the case in the fabricated circuits. A slight phase shift can also be observed which is mainly due to the parasitic effects of the large, manually-soldered circuit.

For the case of the Π network (Fig. 8-(b)), the same discussion above applies with a slightly more evident phase shift. The parasitics on each circuit are different because each circuit has a different layout. Therefore, the phase change, which is mainly due to the parasitics, vary from one design to the other. It can also be observed that the circle of $C_{2,max}$ is slightly distant from the measured boundary, which indicates that the value of $C_{2,max}$ has not been estimated correctly. The maximum value of the capacitance occurs when the bias voltage is low. In such case, the C-V curve experiences an infinite slope as shown in Fig. 6 resulting in an uncertainty in the estimation of the maximum values. Another consequence of this uncertainty is the difference between the maximum limits of the two capacitors even if they are identical due to the effects of the parasitics.

For the case of the Ladder circuit, a very good match between theory and measurements is achieved as shown in Fig. 8 (c). The phase shift in this case is very minor.

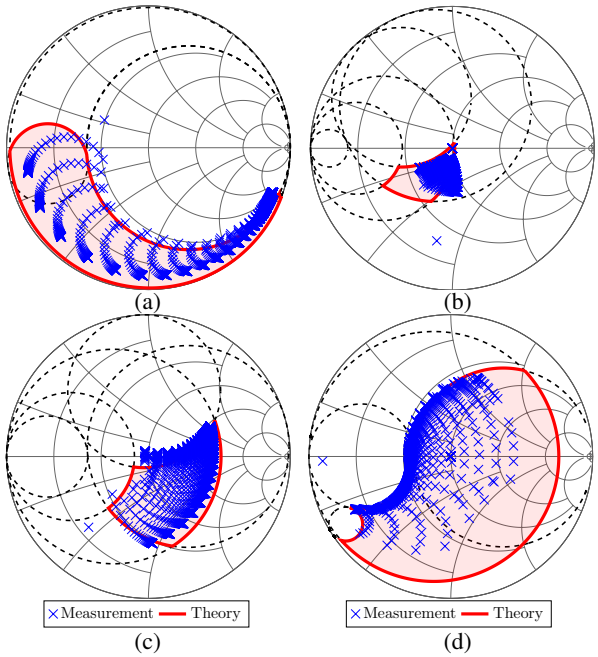

Fig. 8. Measurements of the fabricated prototypes compared with the theory. (a) T-NW. (b) Π-NW. (c) Ladder NW. (d) Hybrid Π NW.

For the hybrid circuit, the comparison has been made at 1 GHz instead of 500 MHz (Fig. 8 (d)) because the size of the lumped circuit is small.

On all the measurements, one or two points can be observed to fall outside of the boundary. These points are found to occur at the lowest bias voltage where the varactor operates on or near its self resonant frequency (SRF) as clear in Fig. 6, which explains the unexpected behaviour.

V. Design Example: Load Modulated PA

As an example of the presented design tool, a PA has been designed with load modulation capability. One of the challenges of PAs is the deterioration of the Power Added Efficiency (PAE) as the power is reduced (backed-off) from its maximum value. This limitation is more serious for applications with high Peak-to-Average Power Ratio (PAPR), where the input signal is considerably backed-off for most of the time. If a tunable MN is used at the output of the PA, the efficiency at power back-off can be increased by varying the output impedance presented to the transistor according to the magnitude of the input signal.

The first step in the design of load-modulated PAs is to identify the optimal output impedances for various input powers. If an accurate transistor-model is available, this task can be achieved by load and source pull simulations. In this work the GaN HEMT transistor CGH40010F from Cree has been used, which has a good simulation model. Load pull simulations have been performed for input power levels from 30 dBm down to 20 dBm (10 dB back-off) at a frequency of 0.8 GHz. The transistor is biased for a class B operation and the second and third harmonics have been optimized for the

maximum power level and kept constant for the other power-values.

The second step is to properly terminate the harmonics. Since they are kept constant in the previous step, a static network between the transistor and the tunable network has been used (Fig. 10). After designing this network, the load-pull data at the transistor plane has been transformed to the tunable network plane as shown in Fig. 10. The transformed trajectory is plotted in Fig. 9 against the coverage of all four network topologies, where the techniques discussed in section III-B have been used. As expected, all four networks can provide the required coverage, but the T-network is chosen due to its lower capacitance-range (Fig. 9-e) and wider coverage.

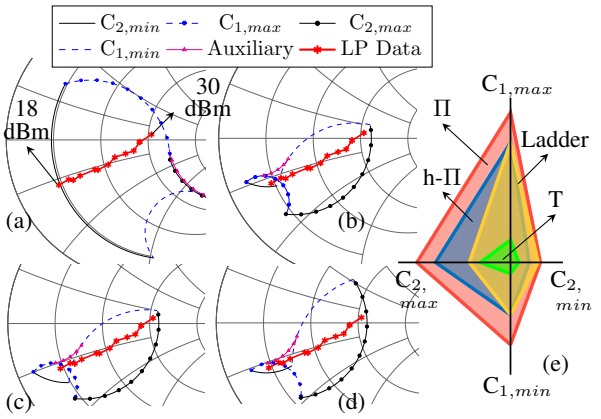

Fig. 9. The coverage of all the networks and the load-pull trajectory (beyond the static NW) of the OMN for input power of 18-30 dBm. (a) T-NW. (b) Π NW. (c) Ladder NW, (d) Hybrid-Π NW. (e) Cost comparison.

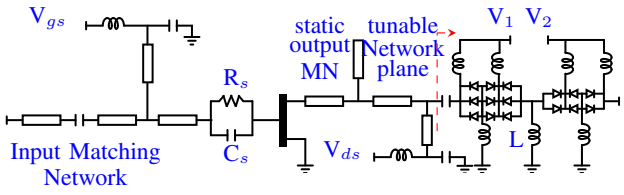

Fig. 10. Schematic of the load-modulated power amplifier with varactors in anti-series configurations.

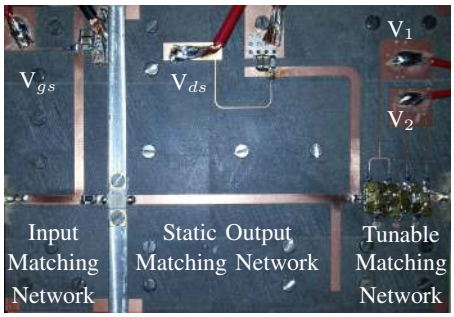

Fig. 11. Photographs of the fabricated power amplifier.

A. Results and Discussion

A prototype amplifier has been fabricated as shown in Fig. 11. The MTV4090 tuning varactor has been used due to its high power handling capability. To increase the power handling even more, the tunable capacitors have been implemented as multiple varactors connected in an anti-series configuration as shown in Fig. 10 and 11.

The PAE is measured at 0.8 and 0.9 GHz for the full dynamic range of the tunable network (V_1 and V_2 between 5 and 70 V). All the measurement has been taken below the 2 dB compression point to maintain a constant gain between 13 and 15 dB. Any measurement resulting in a gain below 13 has been dropped. The results are shown in Fig. 12 where it can be observed that the amplifier achieves a maximum efficiency of 60% and 5 % improvement in the PAE at 10 dBs of power back-off for the case of 0.9 GHz and 2% for the case of 0.8 GHz.

The presented design demonstrates relatively low efficiency improvement, which is due to the losses of the varactors, the package parasitics, and the manual soldering. However, it demonstrates the benefit of the presented theoretical analysis and design guidelines in the design and optimization of tunable PA.

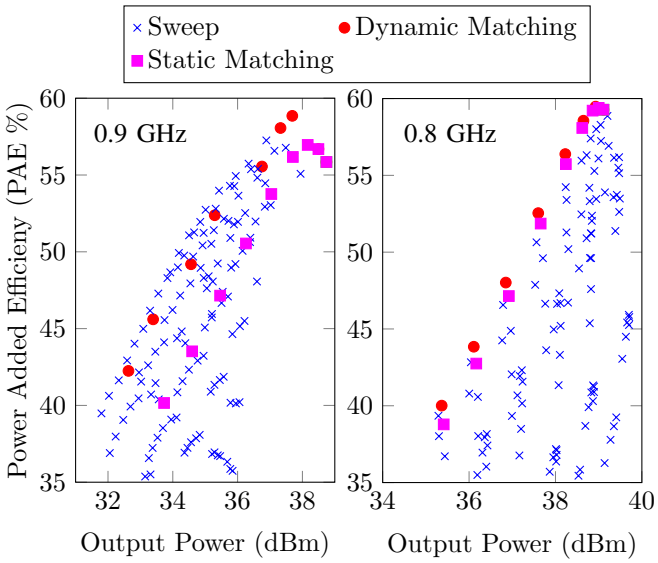

Fig. 12. Measured power added efficiency of the dynamically load modulated power amplifier against the output power at 0.9 GHz and 0.8 GHz. The input power is swept from 20 to 28 dBm and the measured gain is steady at (13-15) dB.

VI. Conclusion

In this work, analytical formulas for the coverage area for four typical matching networks have been derived for the Smith chart for the first time. These theoretical formulas have been validated by circuit simulation and measured results, which agree very well with the theory. The MNs analyzed in this work all have two tuning components (capacitors) and are lossless. Also, only perfect matching is considered. The findings of this work can be extended further by including

the effects of imperfect matching as well as the losses. Nevertheless, the formulas presented here are compact, therefore, suitable for circuit simulators and can be plotted directly on the Smith chart, which enables rapid design of tunable systems. As an example, a load-modulated power amplifier has been designed and tested using the theoretical tools presented in this work.

APPENDIX A
DERIVATION OF THE CENTER AND RADIUS OF AN INNER TANGENTIAL CIRCLE

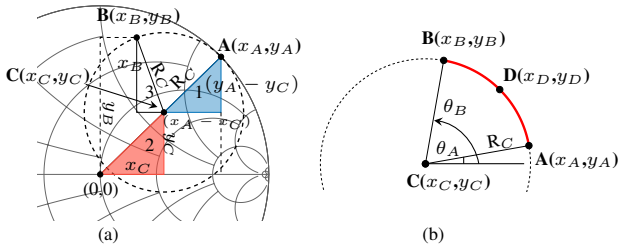

Fig. 13. (a) Illustration of a circle tangential with the $\Gamma = 1$ circle. (b) Illustration of an arc defined by three points together with the center and radius.

In this section the center and radius of a circle tangent to the $|\Gamma| = 1$ circle are derived. The circles are illustrated in Fig. 13-(a), where the tangent point is denoted A(x_A,y_A) and the center is denoted C(x_C,y_C). Point B(x_B,y_B) is any other point on the circle. Triangle 1 and 2 on Fig. 13-(a) are similar, therefore, the ratio of their corresponding sides are in proportion, thus

$$\frac{x_C}{x_A - x_C} = \frac{y_C}{y_A - y_C}$$
$$x_C = \frac{x_A}{y_A} y_C. \tag{26}$$

Evaluating the value of the radius R_C from triangles 1 and 3 and equating them gives:

$$(x_A - x_C)^2 + (y_A - y_C)^2 = (x_B - x_C)^2 + (y_B - y_C)^2$$

$$\begin{aligned}(2x_B - 2x_A)\, x_C + (2y_B - 2y_A)\, y_C \\ = x_B^2 + y_B^2 - x_A^2 - y_A^2.\end{aligned} \tag{27}$$

Substituting form (26) in (27) gives

$$\begin{aligned}\left(\frac{2x_A x_B}{y_A} - \frac{2x_A^2}{y_A} + 2y_B - 2y_A\right) y_C \\ = x_B^2 + y_B^2 - x_A^2 - y_A^2.\end{aligned} \tag{28}$$

Multiplying through by y_A and re-arranging to get y_C as

$$y_C = \frac{y_A \left(x_B^2 + y_B^2 - x_A^2 - y_A^2\right)}{2\left(-x_A^2 - y_A^2 + 2x_A x_B + 2y_A y_B\right)}, \tag{29}$$

and substituting in (26) to get x_C as

$$x_C = \frac{x_A \left(x_B^2 + y_B^2 - x_A^2 - y_A^2\right)}{2\left(-x_A^2 - y_A^2 + 2x_A x_B + 2y_A y_B\right)}. \tag{30}$$

The radius R_C can be calculated directly from triangle 1 as

$$R_C = \sqrt{(x_A - x_C)^2 + (y_A - y_C)^2}. \tag{31}$$

APPENDIX B
DERIVATION OF THE CENTERS AND RADII OF THE AUXILIARY CIRCLES

In this section the value of the capacitor (C_2) that produces the auxiliary circle is derived for all the topologies presented in Fig. 3.

A. Π *Matching Network*

The value of C_2 that gives maximum conductance is referred to as C_2' and can be calculated by first evaluating the real part of the admittance just before the last branch as

$$Y_2 = \frac{(Y_0 + j\omega C_2)\left(\frac{1}{j\omega L}\right)}{Y_0 + j\left(\omega C_2 - \frac{1}{\omega L}\right)}. \tag{32}$$

The real part of which (conductance) can be calculated as:

$$\Re\{Y_2\} = \frac{\cancel{\frac{Y_0 C_2}{L}} + \frac{Y_0}{(\omega L)^2} - \cancel{\frac{Y_0 C_2}{L}}}{Y_0^2 + \left(\omega C_2 - \frac{1}{\omega L}\right)^2}. \tag{33}$$

To evaluate the maximum conductance the derivative of $\Re\{Y_2\}$ with respect to C_2 must be zero, which gives:

$$\frac{2Y_0\left(1 - \omega^2 L C_2'\right)\left(\omega^2 L\right)}{\left(\left(Y_0 \omega L\right)^2 + \left(\omega^2 L C_2' - 1\right)^2\right)^2} = 0. \tag{34}$$

Therefore,

$$1 - \omega^2 L C_2' = 0, \qquad \text{and} \tag{35}$$
$$C_2' = \frac{1}{\omega^2 L}. \tag{36}$$

B. T-Matching Network

In this case, the last branch is a series capacitor (C_1), the forbidden area can be defined by the maximum resistance that can be matched before C_1. The value of C_2' can be calculated by evaluating the real part of the impedance just before the last branch as

$$\Re\{Z_2\} = \Re\{Z_{in}\} = \frac{Z_0 \omega^2 L^2}{Z_0^2 + \left(\omega L - \frac{1}{\omega C_2}\right)^2}. \tag{37}$$

Equating the first derivative with respect to C_2 to zero gives:

$$\frac{\frac{2Z_0 \omega L^2}{C_2'^2}\left(\omega L - \frac{1}{\omega C_2'}\right)}{\left(Z_0^2 + \left(\omega L - \frac{1}{\omega C_2'^2}\right)^2\right)^2} = 0. \tag{38}$$

Since $C_2' = \infty$ can be excluded,

$$C_2' = \frac{1}{\omega^2 L} \tag{39}$$

C. Ladder Matching Network

For this case, a simple transformation can be used to transform Y_0 and L_2 from a series to a parallel configuration. This network can then be analysed in the same way as the Π network. The parallel conductance and susceptance can be calculated to be

$$Y_0' = \frac{Y_0}{1 + (Y_0 \omega L_2)^2} \qquad \text{and} \tag{40}$$

$$B_0 = \frac{-\omega Y_0^2 L_2}{1 + (Y_0 \omega L_2)^2}, \tag{41}$$

respectively. From the results of the Π network in (equation (36)) and assuming that B_0 is capacitive

$$C_2' - \frac{-Y_0^2 L_2}{1 + (Y_0 \omega L_2)^2} = \frac{1}{\omega^2 L_1}, \qquad \text{and} \tag{42}$$

$$C_2' = \frac{1}{\omega^2 L_1} + \frac{Y_0^2 L_2}{1 + (Y_0 \omega L_2)^2}. \tag{43}$$

D. Hybrid Π Matching Network

This network can be analyzed in the same way as the Π network.

$$Y_2 = Y_0 \frac{Y_0 + j\left(\omega C_2 + Y_0 \tan(\theta)\right)}{Y_0 - \omega C_2 \tan(\theta) + j Y_0 \tan(\theta)}, \tag{44}$$

from which the real part can be evaluated as

$$\Re\{Y_2\} = \Re\{Y_{in}\} = \frac{Y_0^3 \left(1 + \tan^2(\theta)\right)}{\left(Y_0 - \omega C_2 \tan(\theta)\right)^2 + \left(Y_0 \tan(\theta)\right)^2}. \tag{45}$$

Applying the maximum conductance condition results in

$$\frac{2 Y_0^3 \omega \tan(\theta) \left[1 + \tan(\theta)\right] \left[Y_0 - \omega C_2 \tan(\theta)\right]}{\left[\left(Y_0 - \omega C_2 \tan(\theta)\right)^2 + \left(Y_0 \tan(\theta)\right)^2\right]^2} = 0, \tag{46}$$

which gives

$$C_2' = \frac{Y_0}{\omega \tan(\theta)}. \tag{47}$$

Appendix C
Plotting an arc knowing its center radius and three points

In this section plotting an arc with a radius of R_C and center C(x_C,y_C) and three points A, B and D is illustrated as shown in Fig. (13(b)). First the angles of the three points are calculated as

$$\theta_i = \tan^{-1}\left(\frac{y_i - y_C}{x_i - x_C}\right), i \in \{A, B, D\} \tag{48}$$

Next, a vector of the ordered (ascending or descending) angles can be formulated as

$$\theta = \left[\theta_A, \theta_2, \theta_3, ..., \theta_k, \theta_D, \theta_{k+2}, ..., \theta_B\right]. \tag{49}$$

The angles in this vector always represent the right arc because they include θ_D. From this vector, the x and y coordinates of any point in the arc can be simply calculated using:

$$x + jy = R_C \left(\cos(\theta) + x_C + j\left[\sin(\theta) + y_C\right]\right). \tag{50}$$

Acknowledgment

This work is supported by the British Engineering and Physical Sciences Research Council (EPSRC), under the FARAD project with grant number EP/M01360X/1 in collaboration with the University of Sheffield, Sheffield, UK.

References

[1] H. Y. Li, C. T. Yeh, J. J. Huang, C. W. Chang, C. T. Yu, and J. S. Fu, "CPW-Fed Frequency-Reconfigurable Slot-Loop Antenna With a Tunable Matching Network Based on Ferroelectric Varactors," *IEEE Antennas and Wireless Propagation Letters*, vol. 14, pp. 614–617, 2015.

[2] H. M. Nemati, C. Fager, U. Gustavsson, R. Jos, and H. Zirath, "Design of Varactor-Based Tunable Matching Networks for Dynamic Load Modulation of High Power Amplifiers," *IEEE Transactions on Microwave Theory and Techniques*, vol. 57, pp. 1110–1118, May 2009.

[3] D. Ji, J. Jeon, and J. Kim, "A Novel Load Mismatch Detection and Correction Technique for 3G/4G Load Insensitive Power Amplifier Application," *IEEE Transactions on Microwave Theory and Techniques*, vol. 63, pp. 1530–1543, May 2015.

[4] J. Kim and J. Jeong, "Range-Adaptive Wireless Power Transfer Using Multiloop and Tunable Matching Techniques," *IEEE Transactions on Industrial Electronics*, vol. 62, pp. 6233–6241, Oct 2015.

[5] T. Lee, "The Smith Chart Comes Home [President's Column]," *IEEE Microwave Magazine*, vol. 16, pp. 10–25, Nov 2015.

[6] C. Sanchez-Perez, J. de Mingo, P. L. Carro, and P. Garcia-Ducar, "Design and Applications of a 300 - 800 MHz Tunable Matching Network," *IEEE Journal on Emerging and Selected Topics in Circuits and Systems*, vol. 3, pp. 531–540, Dec 2013.

[7] V. Freitas, J. D. Arnould, and P. Ferrari, "General Expression for Tunable Matching Network Efficiency in the case of complex impedances," in *Microwave Optoelectronics Conference (IMOC), 2013 SBMO/IEEE MTT-S International*, pp. 1–5, Aug 2013.

[8] V. Freitas, J.-D. Arnould, and P. Ferrari, "General expression for tunable matching network efficiency in the case of complex impedances," *Microwave and Optical Technology Letters*, vol. 57, no. 5, pp. 1160–1166, 2015.

[9] C. Hoarau, N. Corrao, J. D. Arnould, P. Ferrari, and P. Xavier, "Complete Design and Measurement Methodology for a Tunable RF Impedance-Matching Network," *IEEE Transactions on Microwave Theory and Techniques*, vol. 56, pp. 2620–2627, Nov 2008.

[10] M. Schmidt, E. Lourandakis, A. Leidl, S. Seitz, and R. Weigel, "A comparison of tunable ferroelectric Π;- and T-matching networks," in *Microwave Conference, 2007. European*, pp. 98–101, Oct 2007.

[11] F. C. W. Po, E. de Foucauld, D. Morche, P. Vincent, and E. Kerherve, "A Novel Method for Synthesizing an Automatic Matching Network and Its Control Unit," *IEEE Transactions on Circuits and Systems I: Regular Papers*, vol. 58, pp. 2225–2236, Sept 2011.

[12] P. Sjblom and H. Sjland, "Constant Mismatch Loss Boundary Circles and Their Application to Optimum State Distribution in Adaptive Matching Networks," *IEEE Transactions on Circuits and Systems II: Express Briefs*, vol. 61, pp. 922–926, Dec 2014.

[13] M. Thompson and J. K. Fidler, "Determination of the impedance matching domain of impedance matching networks," *IEEE Transactions on Circuits and Systems I: Regular Papers*, vol. 51, pp. 2098–2106, Oct 2004.

[14] Y. Sun and J. Fidler, "Determination of the impedance matching domain of passive {LC} ladder networks: Theory and implementation," *Journal of the Franklin Institute*, vol. 333, no. 2, pp. 141 – 155, 1996.

[15] J. K. Fidler and Y. Sun, "Computer-aided determination of impedance matching domain," in *IEE Twelfth Saraga Colloquium on Digital and Analogue Filters and Filtering Systems*, pp. 1/1–1/6, Nov 1992.

[16] R. Ludwig and P. Bretchko, *RF Circuit Design: Theory and Applications*. No. v. 1 in RF Circuit Design: Theory and Applications, Prentice-Hall, 2000. pp.415-416.

Eyad Arabi (S'14, M'15) received his M.Sc. and Ph.D. in electrical engineering from Chalmers University of Technology, Göteborg, Sweden and King Abdullah University of Science and Technology (KAUST), Thuwal, Saudi Arabia, respectively. Since August 2015 he is working as a research associate with the Communication Systems and Networks (CSN) research group, the University of Bristol, Bristol, UK.

His current research interests include tunable and multi-band power amplifiers and filters for frequencies below 6 GHz for the fifth generation mobile networks.

Kevin A. Morris received the B.Eng. and Ph.D. degrees in electronics and communications engineering from the University of Bristol, Bristol, U.K., in 1995 and 2000, respectively. He is currently a Reader of RF engineering and Head of the Department of Electrical and Electronic Engineering, University of Bristol. He has authored or coauthored over 80 academic papers. He holds five patents. His research interests principally concern looking at methods of reducing power consumption in communications systems including the area of RF hardware design with a specific interest in the design of efficient linear broadband power amplifiers for use within future communications systems. Dr. Morris is currently involved with a number of the Engineering and Physical Sciences Research Council (EPSRC) including FARAD and SENSE and Industry funded research programs within the U.K

Mark A. Beach received his PhD for research addressing the application of Smart Antenna techniques to GPS from the University of Bristol in 1989, where he subsequently joined as a member of academic staff. He was promoted to Senior Lecturer in 1996, Reader in 1998 and Professor in 2003. He was Head of the Department of Electrical & Electronic Engineering from 2006 to 2010, and then spearheaded Bristols hosting of the EPSRC Centre for Doctoral Training (CDT) in Communications. He currently manages the delivery of the CDT in Communications, leads research in the field of enabling technologies for the delivery of 5G and beyond wireless connectivity, as well as his role as the School Research Impact Director. Marks current research activities are delivered through the Communication Systems and Networks Group, forming a key component within Bristols Smart Internet Lab. He has over 25 years of physical layer wireless research embracing the application of Spread Spectrum technology for cellular systems, adaptive or smart antenna for capacity and range extension in wireless networks, MIMO aided connectivity for through-put enhancement, Millimetre Wave technologies as well as flexible RF technologies for SDR modems underpins his current research portfolio.